An alternative approach to model mechanical stress effects on magnetic hysteresis in electrical steels using complex permeability

A.P.S. Baghel, B Sai Ram, L. Daniel, S.V. Kulkarni, G. Krebs, J.B. B
Blumenfeld, L. Santandrea

HAL Id: hal-02504848

https://centralesupelec.hal.science/hal-02504848

Submitted on 22 Oct 2021

An Alternative Approach to Model Mechanical Stress Effects on Magnetic Hysteresis in Electrical Steels using Complex Permeability

A. P. S. Baghel[a,b], B. Sai Ram[a], L. Daniel[b], S. V. Kulkarni[a], G. Krebs[b], J. B. Blumenfeld[c], L. Santandrea[b]

[a]Department of Electrical Engineering, Indian Institute of Technology Bombay, Mumbai, 400076, India
[b]Group of Electrical Engineering - Paris (GeePs), UMR CNRS 8507, CentraleSupélec, Univ. Paris-Sud, Université Paris-Saclay, Sorbonne Université, 3 & 11 rue Joliot-Curie, Plateau de Moulon 91192 Gif-sur-Yvette Cedex, France
[c]Renault, 1 avenue du Golf, 78288 Guyancourt, France

Abstract

The presence of mechanical stress significantly affects the performance of electrical machines, particularly in terms of permeability and losses of core materials. A precise modeling of electrical machines requires to consider such magneto-elastic couplings. An efficient approach needs a constitutive model to predict magneto-elastic hysteretic characteristics and its implementation into numerical analyses. However, it is a challenging task for engineers and researchers due to computational time and convergence issues. This paper deals with an approach to model the magneto-elastic behavior of electrical steels using complex permeability. The complex permeability function is used in this work for the first time in the literature to model the effects of stress. The proposed model is quite amenable to numerical analyses and it reduces computational time significantly. Although, the proposed approach is applicable to steady state or cyclic fields and it considers only reversible effects of stress. It provides an alternative way to consider magneto-elastic coupled behavior in numerical analysis of electrical devices involving magnetic materials. Computed results are in good agreement with measured ones with a maximum error of 2.5 % for different stress levels and frequencies.

Keywords: Electrical steel, complex permeability, magneto-elastic behavior, iron loss, finite element method

1. Introduction

Magnetic properties of ferromagnetic materials, used in magnetic circuits of electrical machines, are strongly affected by mechanical stress which affects particularly permeability and losses of core materials [1]-[2]. In high-speed applications, due to design constraints (compact design and reduced weight), the core materials generally have more exposure to mechanical stresses [3]-[4]. Other main causes of induced mechanical stress in the iron sheets are manufacturing processes (e.g. cutting or stamping), assembly processes (e.g. shrink-fitting), temperature gradients, and centrifugal forces [5]-[6]. Core losses are more affected by compressive stress than tensile stress [7]. As an illustration, the effect of mechanical stress on the magnetic properties of a non-oriented (NO) material is shown in Fig. 1.
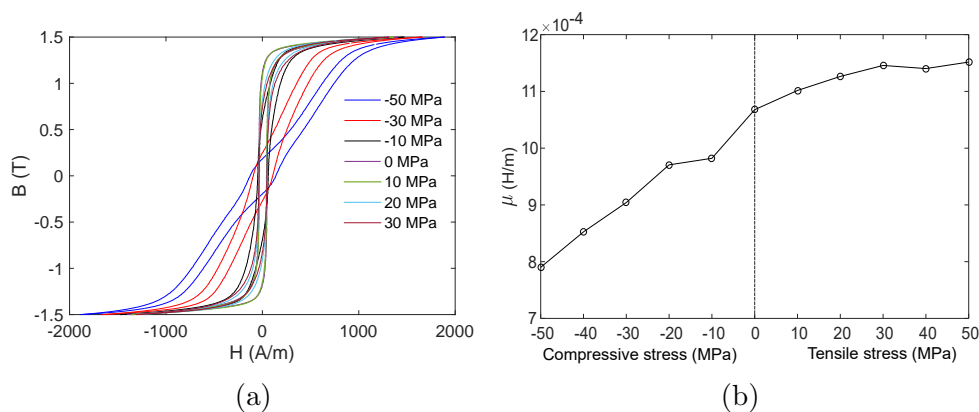

Figure 1: Variation of (a) Hysteresis loops at 1.5 T, 50 Hz for different stresses levels [7] (b) Permeability at different stress levels at 1.5 T, 50 Hz

The magneto-elastic behaviour of ferromagnetic materials plays a significant role in the performance of electrical machines [8], [9], [10], because of change in magnetic properties of electrical steel [11]. The accuracy of loss computation is significantly affected if the analysis is performed without considering stress effects [8].

Computational time and accuracy are two important aspects that need to be considered during the design and analysis of electrical machines [12]. A significant amount of research has been done on the estimation of iron losses in electrical machines subjected to mechanical stress [3], [4], [13], [14], [15], [16] but major issues remain, viz. lack of predictive hysteretic constitutive magneto-mechanical model and complex numerical implementation.

2

Numerous hysteresis models for ferromagnetic materials are available in the literature [17], [18], [19]. Among them Preisach formalism and Jiles-Atherton (JA) model are widely used. Most of the existing magneto-mechanical coupled models are built as extensions of these classical magnetic hysteresis models. Preisach models have been modified for consideration of stress-effects through their distribution functions [20], [21], [22], [23]. On the other hand, the JA model has been extended in order to consider magneto-elastic effects using the concept of effective field [23], [24], [25], [26]. Another model based on a multi-scale approach, derived through the energy equilibrium for the description of anhysteretic magnetization, has been proposed [27]. The model is successful in describing the magneto-elastic coupled behaviour of ferromagnetic materials [28]. Implementation of complete hysteresis models in Finite Element Method (FEM) simulations is known as intrinsic approach [3], [29], [30]. Since the approach considers comprehensive hysteretic descriptions, it is a realistic description and very accurate to calculate losses directly in the FEM formulation. However, numerical implementation of these models leads to high computational burden and it poses serious convergence issues [3], [30]. Another approach is to decouple the single-valued non-linear curve (anhysteretic curve) for use in field analysis (FEM) and to compute the loss at the post-processing stage using an appropriate loss formula [31], [32], [33]. This approach is known as a posteriori approach. A significant number of papers are reported in the literature, which have used this approach in order to consider stress effects [34], [35], [36], [37]. This approach shows reduced computational time and simpler convergence properties compared to the intrinsic approach (implementation of complete magneto-elastic hysteresis model). However, the approach does not consider hysteresis effects in the FEM formulation itself, which may affect its accuracy.

Another interesting methodology to describe magnetic properties is a complex permeability based approach [38], [39]. In this methodology, non-linear hysteretic properties of core materials are represented by elliptic (or linear) loops using complex permeability [39]. Applied first without considering the effect of stress, the approach leads to a huge reduction in computational time and shows no convergence issues due to its linear nature. It provides a way to represent magnetic characteristics of the core material as a function of frequency [40]. Therefore, the approach is frequently used in high-frequency analysis such as sweep frequency response analysis (SFRA) of power transformers [40], [41], [42]. The computation of equivalent complex permeability can be done using two approaches. The first method considers

3

a fundamental harmonic component of B and phase difference between B and H as the hysteresis loss angle, and this approach is called Fundamental Harmonic Method (FHM) [38]. The second method considers core losses to compute the imaginary part of the equivalent complex permeability and it also retains the exact values of B_{max} and H_{max} of the hysteresis loop. This method is known as the equivalent core loss (ECL) approach [39].

This paper aims at offering a simple equivalent complex permeability approach to designers and researchers for the estimation of losses in electrical machines subjected to significant mechanical stress levels. The present analysis here is restricted to model the effect of mechanical stresses in elastic range. The approach consists of modification of tanh representation of complex permeability derived from Maxwell's equations. The effects of mechanical stress are modeled using the equivalent complex permeability by representing its real and imaginary part as a function of the stress. The non-linear stress dependence of the complex permeability can be determined using measured loss data at two different stress levels. The paper also discusses computation of equivalent complex permeability using reluctivity with prior knowledge of induction B instead of H, which is often the case in numerical simulations (FEM) and standard measurement systems. The proposed approach is first compared with conventional approaches using FEM simulation of single sheet tester (SST) at zero stress condition, and it is found to give comparable accuracy with significant reduction in computational time. Thereafter, the approach is applied for loss computation over a range of compressive and tensile stress levels (up to 50 MPa). The computed losses are in close agreement with measured ones.

2. Complex Permeability Representation of Magnetic Characteristics

The magnetic permeability of a material defines its ability to get magnetized. For a ferromagnetic material, the hysteresis losses can be represented in terms of phase difference (θ_l) between B and H. This phenomenon is represented by a delay in the response (B) to the excitation (H) and thus, B lags H by angle θ_l, [43]. By considering B and H in the phasor form, the permeability can be defined in complex notations as:

$$\mu_l = \frac{B}{H} = \mu e^{-j\theta_l} = \mu' - j\mu'' \tag{1}$$

4

In addition to the hysteresis loss, in the presence of time-varying magnetic fields, dynamic losses (classical eddy current and excess losses) make the complex permeability frequency-dependent [38]. The effective frequency-dependent complex permeability is derived from the diffusion equation for a semi-infinite single sheet (as shown in Fig. 2) as:
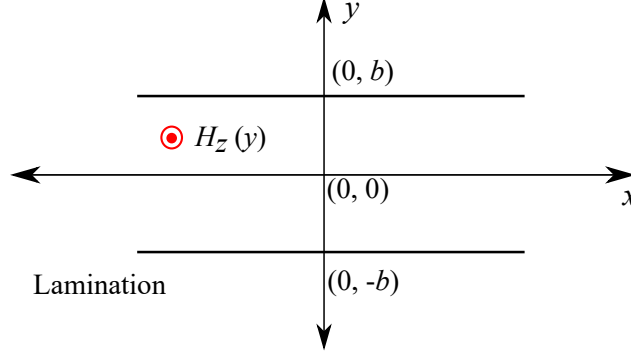

Figure 2: Semi-infinite single sheet in z-direction with x dimensions much greater than the y dimensions

$$\nabla^2 \mathbf{H} = j\omega\mu_l\sigma\mathbf{H} \tag{2}$$

Here, σ is the electric conductivity of the magnetic material and ω is the angular frequency of the excitation. In the figure, the magnetic field in the z-axes varies along the y-direction.

Thus, eq. 2 can be solved as:

$$\frac{\partial^2 H_z}{\partial z^2} = \alpha^2 H_z \implies H_z = A_1 e^{\alpha y} + A_2 e^{-\alpha y} \tag{3}$$

Here, $\alpha^2 = j\omega\sigma\mu_l \implies \alpha = \sqrt{j\omega\sigma\mu_l} = (1+j)\sqrt{j\omega\sigma\mu_l/2} = (1+j)/\delta$, and by applying boundary conditions as $(H_z(b) = H_z(-b) = H_{max})$ for the lamination in Fig. 2, eq. 3 can be reduced to

$$H_z = H_{max}\frac{\cosh y}{\cosh b} \tag{4}$$

Using eq. 1 and eq. 4, the effective complex permeability (μ_{eff}) can be

calculated using the average magnetic flux density (B_{avg}) as given below:

$$\mu_{eff} = \mu' - j\mu'' = \frac{B_{avg}}{H_{max}} = \frac{1}{H_{max}2b} \int_{-b}^{b} \mu_l H_z(y) dy$$
$$= \mu_l \frac{\tanh \alpha b}{\alpha b} = \mu_l \frac{\tanh(1+j)b/\delta}{(1+j)b/\delta} \tag{5}$$

In the above equation, α, δ are propagation constant and skin depth of electromagnetic field inside a conductor [44], [45], respectively. These parameters depend on permeability and conductivity of the material and on the frequency. Equation 5 can be used to model the effective complex permeability as a function of frequency. The parameter (μ_l) is derived by using μ_{eff} values calculated from hysteresis loops at different frequencies, the maximum magnetic field H_{max} being constant [38].

However, practical situations might be different since standard measurement systems usually set a maximum value of the magnetic induction B_{max} which is maintained constant for measurements at different frequencies. In this case, the effective complex permeability is calculated in terms of reluctivity using the energy loss. For a sinusoidal flux density (B), the energy loss (P) per cycle is:

$$P = \int_T H(B) dB = \int_T H(B) \frac{dB}{dt} dt \tag{6}$$

The flux density can be written as:

$$B = B_{max} e^{j\omega t} \tag{7}$$

$$\frac{dB}{dt} = j\omega B_{max} e^{j\omega t}$$

The magnetic field intensity (H) can be computed as:

$$H = real(\nu_c B) = (\nu' + \nu'') B_{max} e^{j\omega t} = B_{max}(\nu' \cos \omega t + \nu'' \sin \omega t) \tag{8}$$

Substituting eq. 7 and eq. 8 in eq. 6 and integrating over one time period, yields

$$\nu'' = \frac{P}{\pi B_{max}^2} \tag{9}$$

Using the relations $H_{max} = |\nu| B_{max} \implies |\nu| = \frac{H_{max}}{B_{max}}$, the real part of reluctivity can be computed as:

$$\nu' = \sqrt{|\nu|^2 - \nu''^2} \tag{10}$$

6

Using eq. 9 and eq. 10, the complex reluctivity is determined using three frequency-loss data sets (here, loss data at 50, 1000, 2000 Hz are used) in order to compute the frequency-dependent effective complex permeability. Hence, non-linear hysteretic characteristics are basically transformed into linear-elliptical hysteretic loops using the complex permeability approach as shown in Fig. 3.
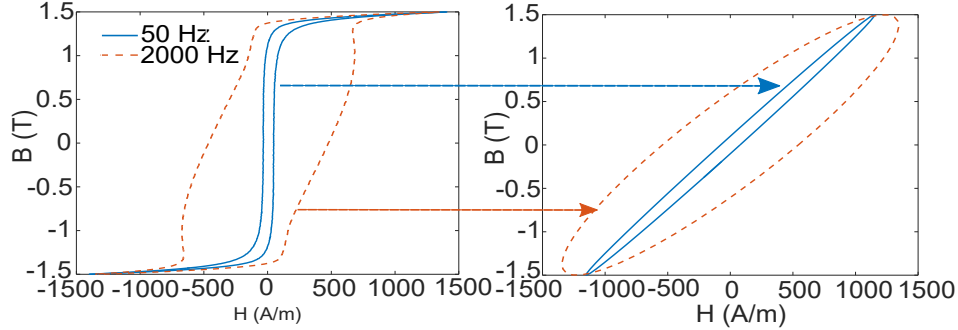

Figure 3: Conversion of non-linear hysteresis characteristics to linear-elliptical hysteresis loops at 1.5 T

3. Modeling of Stress Effects using Complex Permeability

Magneto-mechanical characteristics of ferromagnetic materials can be modeled using the frequency dependent complex permeability function derived in Section 2. First, the effective complex permeability can be computed using the components of complex reluctivity (eq. 9 and eq. 10) at each stress level. Thus, the real and imaginary parts of the complex permeability are made to change with the stress level. The phasor representation of the effect of stress on B, H and ν is shown in Fig. 4. In the figure, the magnetic flux density is kept constant. In the phasor representation, $\sigma_{s1} < \sigma_{s2}$ for compressive stress and $\sigma_{s1} > \sigma_{s2}$ for tensile stress.

Under compressive stress the hysteresis loop generally bends as shown in Fig. 1 and higher H is required (as evident in Fig. 4) to setup a given flux density, and therefore the real part of complex permeability decreases as shown in Fig. 1b. Thus, the phase angle θ_{eff} between B and H increases as the stress increases from σ_{s1} to σ_{s2} as shown in Fig. 4. However, in case of tensile stress, the hysteresis loops straightens about vertical axis and so the required H will be lower to setup a given B and the phase angle (θ_{eff}) decreases with increase in stress.
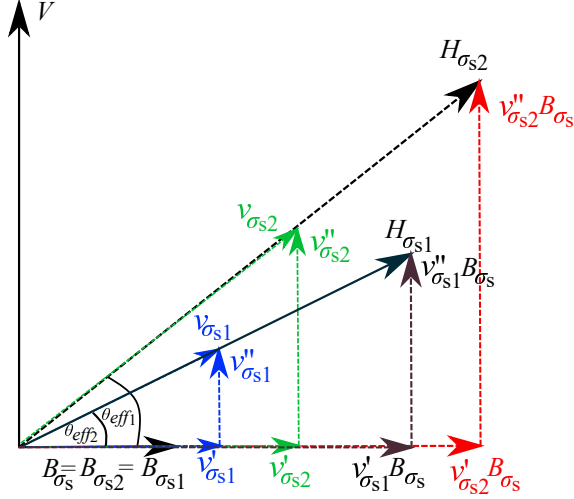
7

In the frequency-dependent complex permeability function eq. 5, the stress effects can be included through μ_l to represent these effects on the losses and permeability [7]. The variations of real and imaginary parts of μ_l with stress are shown in Fig. 5. Both real and imaginary parts μ_{lr} and

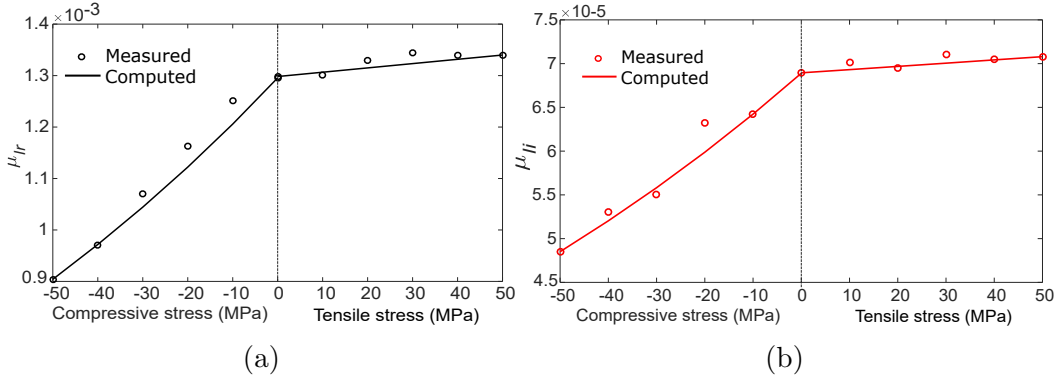(a)

(b)

μ_{li} decrease as the compressive stress increases. On the other hand they increase as the tensile stress increases. The following exponential function can be used to model the variation of μ_l for both compressive and tensile

stress conditions:

$$\mu_{lr} = \mu_{lr0}e^{a_r\sigma_s} \tag{11a}$$

$$\mu_{li} = \mu_{li0}e^{a_i\sigma_s} \tag{11b}$$

Here μ_{lr0} and μ_{li0} are the real and imaginary part of μ_l at the zero stress condition. σ_s is positive for tensile stress and negative for compressive stress. a_r and a_i are constants describing the behaviour of the real and imaginary parts of the effective complex permeability with stress and their values are different for compressive and tensile stresses. These coefficients can be determined using loss-data sets at two stress levels. Here, the loss data sets at 0 and $+/-50$ MPa stress levels are chosen to determine these parameters for both type of stress levels (compressive (0 and -50 MPa) and tensile (0 and 50 MPa)). The effective complex permeability as a function of frequency and stress can be written as:

$$\mu_{eff}(\sigma_s, \omega) = \mu_l(\sigma_s)\frac{\tanh \alpha b}{\alpha b} \tag{12}$$

where, $\alpha = \sqrt{j\omega\mu_l(\sigma_s)\sigma}$ and the variation of complex permeability as a function of compressive stress and frequency is shown in Fig. 6. From the figure, one can infer that the variation of frequency dependency of real and imaginary parts of complex permeability is significant for compressive stress (Fig. 6a). In case of tensile stress (Fig. 6b), a notable change is not observed for real and imaginary parts of complex permeability. The elliptic hysteresis
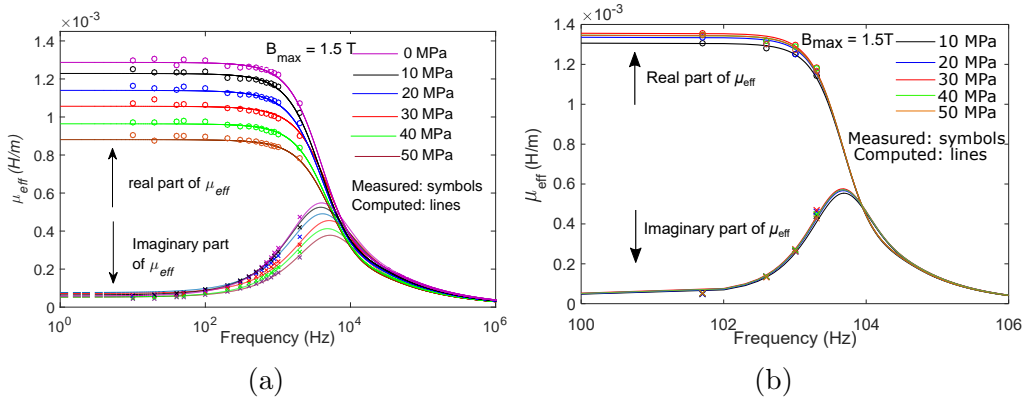

Figure 6: Variation of complex permeability at 1.5 T as a function of frequency at different stress levels (a) compressive stress (b) tensile stress

9

loops at 1.5 T for frequencies 50 Hz and 2 kHz with different stress levels is shown in Fig. 7.
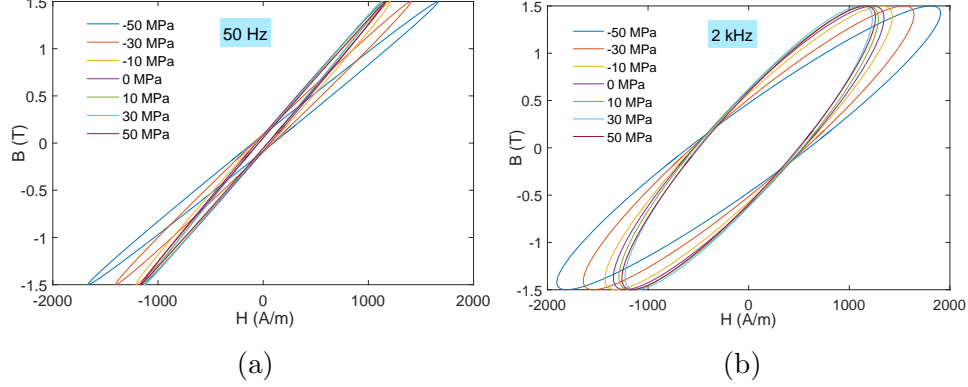
4. FEM Implementation of the Proposed Magneto-elastic Complex Permeability

Hysteresis loops and corresponding losses are measured for non-oriented electrical steel; grade-M235-35A using a single sheet tester (SST). The measurement setup comprises a pneumatic tension and compression unit as shown in Fig. 8a. Thickness and conductivity of laminations used for measurement are $2b = 0.33$ mm and $\sigma = 2.08\times10^6$ S/m. The performance of the suggested approach is first determined using other approaches (a posteriori and full hysteresis implementation-intrinsic approach) for the zero-stress (unloaded) condition. Then, the magneto-elastic complex permeability is applied to the loss computation in a stressed (loaded) condition by simulating the SST device. The geometry of the setup is shown in Fig. 8b.

4.1. Intrinsic approach

In this approach, the JA model is integrated into the FEM formulation. The governing field equation is [46]:

$$\frac{1}{\mu}(\frac{\partial^2 A}{\partial x^2} + \frac{\partial^2 A}{\partial y^2}) = -J_o = -\frac{NI}{S} \tag{13}$$
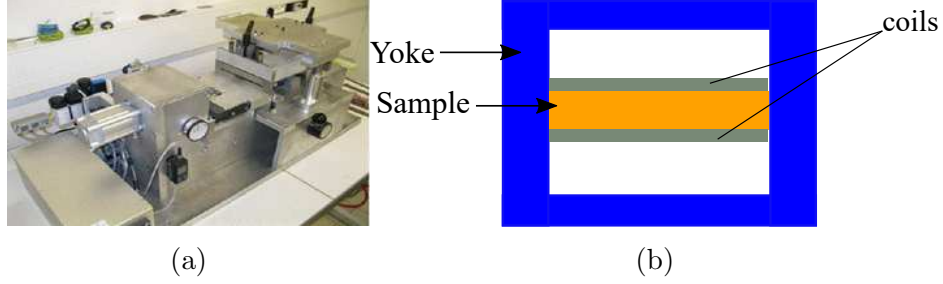
10

where, S and N are the cross-sectional area and the number of turns of the winding, respectively. The circuit equation can be written as:

$$U = \frac{d}{dt}\phi + [R_{ext}]I + \frac{d}{dt}[L_{ext}]I \tag{14}$$

In the above equations, U is the supply voltage, I is the current drawn, A is the magnetic vector potential, S is the cross-sectional area of the conductor, and ϕ is the magnetic flux linkages with the winding. R_{ext} and L_{ext} are the resistance and inductance of the winding and, μ is a non-linear function of B, calculated using a hysteresis model. In FEM formulation, the final field and circuit equations can be written as [39]:

$$[K][A] + [T]\frac{d}{dt}[A] + [D][I] = 0 \tag{15a}$$

$$[D]'\frac{d}{dt}[A] + [R_{ext}][I] + [L_{ext}]\frac{d}{dt}[I] = U \tag{15b}$$

The non-linear solver uses the local coefficient method (LCM) in the fixed-point approach [47].

In the above equation, $[K]$ represents the global coefficient matrix, $[T]$ and $[D]$ correspond to the eddy current term and the source term respectively [46]. For material modeling, hysteresis loops are approximated using the JA model in this analysis [39].

In the JA model, the minimum energy state of magnetic materials can be represented using the anhysteretic magnetization [17]. It is defined in terms of three parameters, a, α, and M_s as:

$$M_{an} = M_s[\coth(\frac{H_e}{a}) - \frac{a}{H_e}] \tag{16}$$

11

Table 1: Optimized JA parameters

Parameter	Optimized values
M_s	1.22×10^6 A/m
a	85 A/m
k	70 A/m
α	2.0×10^{-4}
c	0.1

where, M_{an}, is the anhysteretic magnetization. H_e is the effective field and it can be written as:

$$H_e = H + \alpha M \tag{17}$$

where, M and H are the total magnetization and the applied magnetic field.

The hysteretic behavior is obtained using the energy balance principle with reversible and irreversible magnetization components [17]. It can be represented in its inverse form by the following differential equation [30]:

$$\frac{dM}{dB} = \frac{(1-c)\frac{dM_{irr}}{dB_e} + \frac{c}{\mu_o}\frac{dM_{an}}{dH_e}}{1 + c(1-\alpha)\frac{dM_{an}}{dH_e} + \mu_o(1-c)(1-\alpha)\frac{dM_{irr}}{dB_e}} \tag{18}$$

where, B and M_{irr} are the flux density and the irreversible magnetization, μ_o is the free space magnetic permeability, and δ is the directional parameter with the value +1 for $dH/dt > 0$ and -1 for $dH/dt < 0$. The model is applied on a measured hysteresis loop (1.5 T, 50 Hz) of a non-oriented material (M235-35A) sample. Optimized parameters are given in Table 1. The surface plot of flux density (in the sample) and the computed current waveform are shown in Fig. 9.

4.2. A posteriori approach

In this approach, FEM analysis is carried out using the anhysteretic curve and the total losses are calculated at the post-processing stage [33]-[31]. The loss model is given as [31]-[32]:

$$P = k_h f B_{max}^2 + k_e f^2 B_{max}^2 + k_{ex} f^{1.5} B_{max}^{1.5} \tag{19}$$

Here, k_h, k_e, and k_{ex} are the hysteresis, classical eddy current and excess loss coefficients respectively. B_{max} and f are the peak induction value and frequency respectively. The loss coefficients can be determined using measured
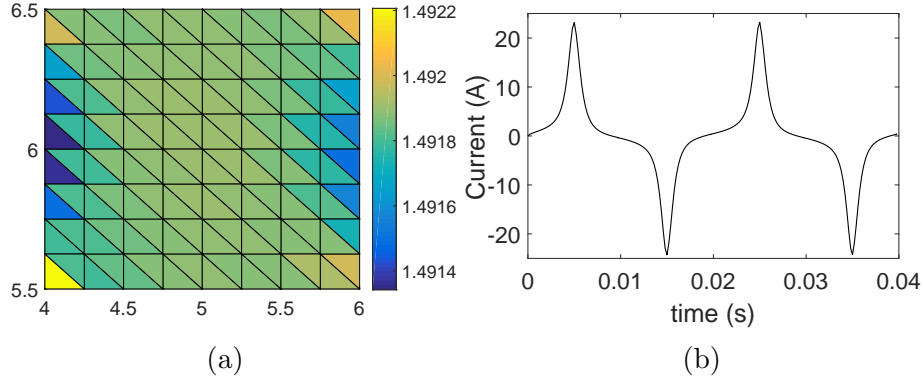
12

Figure 9: Simulation results (a) surface plot of flux density of the sample region shown in Fig. 8b (b) the computed current waveform

loss-frequency data. The FEM analysis is performed with an anhysteretic curve, determined from the JA model as given in *intrinsic approach*.

4.3. FEM analysis using complex permeability approach

A time-harmonic analysis is used involving complex permeability and the loss is computed by the area of the elliptic $B - H$ loop. The final FEM equation can be obtained from eq. 13 and eq. 14 as [40]:

$$[K][A] + j\omega[T][A] + [D][I] = 0 \tag{20a}$$

$$j\omega[D]'[A] + [R_{ext}][I] + j\omega[L_{ext}][I] = [U] \tag{20b}$$

Here, the elements of the K matrix are complex quantities and eq. 20 is solved in the frequency domain. The surface plot and line plots of magnetic flux density are shown in Fig. 10.

4.4. Comparison of the three approaches

The performance of the three approaches discussed previously can be compared in terms of accuracy and computational time, as given in Table 2. The accuracy of the complex permeability is reasonably comparable to the intrinsic approach. Also, a huge reduction in computational time is obtained by using the complex permeability approach.

The approach can now be applied to compute losses under mechanical stress conditions using the magneto-elastic complex permeability given by eq. 12. The loss is computed at 1.5 T for a frequency from 10 Hz up to 2 kHz.
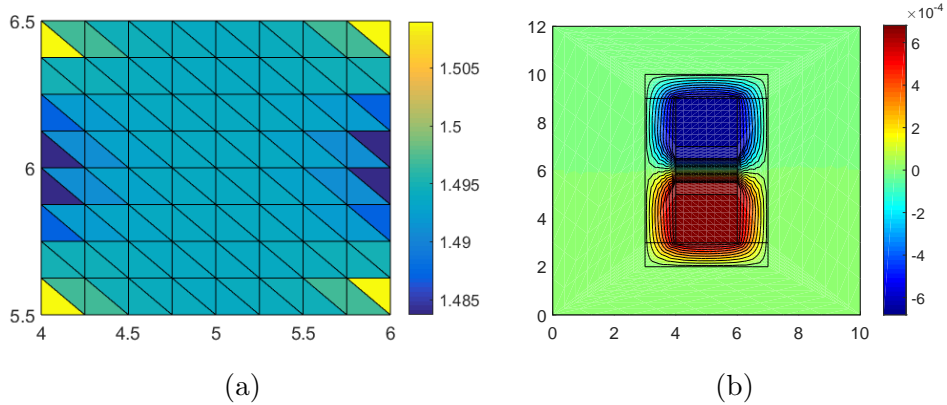
13

Figure 10: Simulation results (a) surface plot of flux density of the sample region shown in Fig. 8b (b) flux lines

Table 2: Comparison of three approaches

Approaches	Computed values (W/kg)	Measured values (W/kg)	computational time (s)
Intrinsic approach	2.20	2.28	1891
Extrinsic approach	2.17	2.28	450
Complex permeability	2.40	2.28	2

4.5. Results and discussion

FEM simulations of the SST device are carried out for each stress level using the stress-dependent complex permeability. Computed and measured losses for different compressive and tensile stress levels are shown in Fig. 11. Maximum error among all stress levels at different frequencies is around 2.5 %. Model parameters for 1.5 T for compressive and tensile stresses are given in Table 3. The same method is also carried out to compute losses for maximum induction levels of 0.5 T and 1.0 T (given in Figs. 12 and 13). Since the compressive stress affects the core loss more significantly than the tensile stress, these analyses are performed only for compressive stress levels. Model parameters for these induction levels are given in Table 4.

The magneto-elastic model using complex permeability can be repre-

14

Table 3: Parameters of complex permeability model for $B_{max} = 1.5$ T

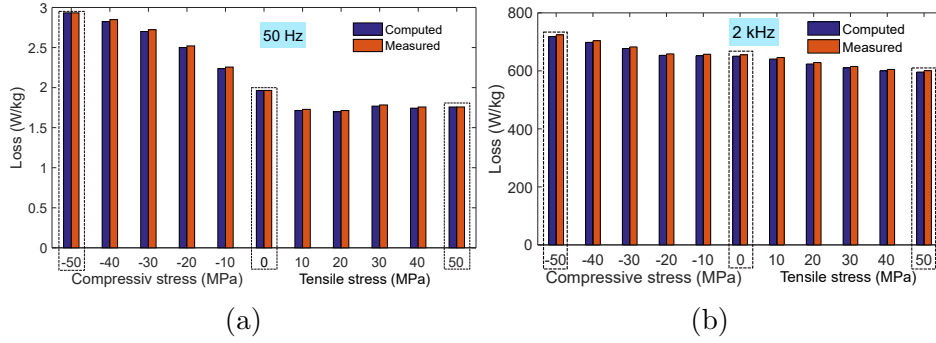| Type of stress	μ_{lr0}	μ_{li0}	a_r (MPa^{-1})	a_i (MPa^{-1})
Compressive $(\sigma < 0)$	0.0013	6.89×10^{-5}	6.52×10^{-9}	7.19×10^{-9}
Tensile $(\sigma > 0)$	0.0013	6.89×10^{-5}	6.0611×10^{-10}	4.591×10^{-10}

Figure 11: Comparison of measured and calculated loss using time-harmonic FEM for induction level of 1.5 T (a) 50 Hz (b) 2 kHz

sented using a simple function of stress over a wide range of frequencies. The model involves very few parameters, and hence it needs less measured data for parameter identification process which is straightforward. The magneto-elastic effects can be considered in the FEM analysis of electrical machines using the proposed approach. The present approach is isotropic, which particularly ignores stress-induced anisotropy since the magnetic permeability is described as a scalar. However, the anisotropy can be introduced using a tensor form of the effective complex permeability as reported in [45]. Moreover, the approach has been applied to simple configurations with uniaxial loading. If the loading is multi-axial, the present approach can be used with

Table 4: Parameters of complex permeability model for different induction levels and compressive stresses

Induction level	μ_{lr0}	μ_{li0}	a_r (MPa^{-1})	a_i (MPa^{-1})
0.5 T	0.012	0.0105	4.47×10^{-8}	7.73×10^{-8}
1.0 T	0.0116	6.5×10^{-3}	4.32×10^{-8}	7.42×10^{-8}

15

Figure 12: Comparison of measured and calculated loss using time-harmonic FEM for induction level of 0.5 T (a) 50 Hz (b) 500 Hz (c) 2 kHz

equivalent uniaxial stress derived from the equivalence between 2D and 1D magnetostrictive energies [48], [49].

5. Conclusion

This paper is devoted to the modeling of magneto-elastic properties of electrical steels using a complex permeability approach. In this work a frequency-dependent tanh function for complex permeability, derived using Maxwell's equations, has been improved to consider magneto-mechanical effects. Complex permeability has been calculated using reluctivity which is
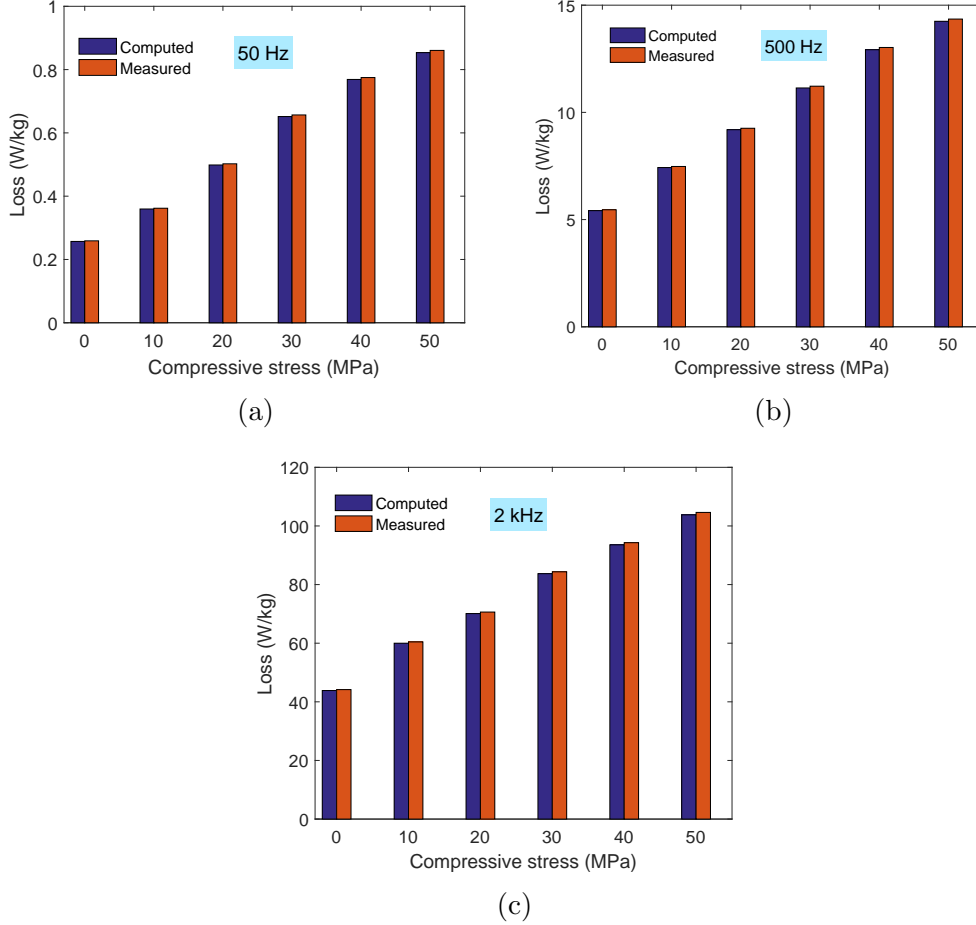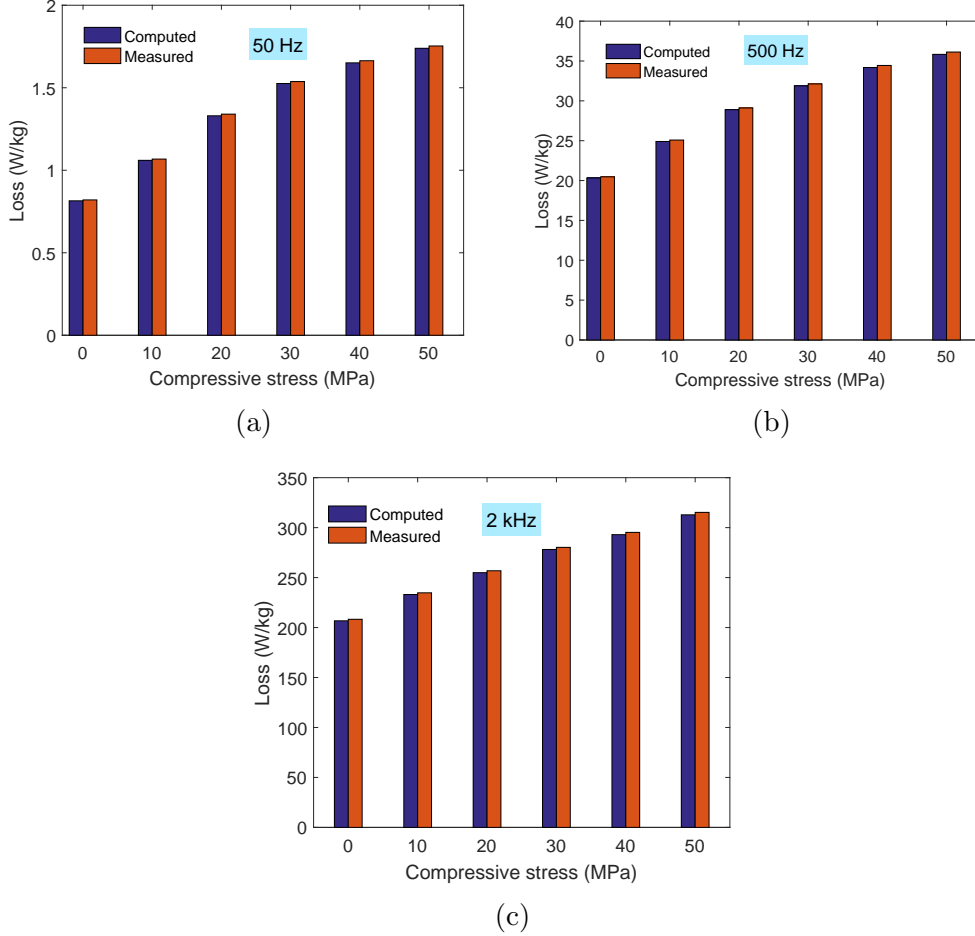
Figure 13: Comparison of measured and calculated loss using time-harmonic FEM for induction level of 1.0 T (a) 50 Hz (b) 500 Hz (c) 2 kHz

determined using energy loss. The magneto-mechanical effects on permeability and losses are incorporated in the complex permeability. The presented work compares the proposed approach with the conventional intrinsic and a posteriori approaches using the FEM modeling of a single sheet tester under the unloaded condition. The work also discusses the computation of equivalent complex permeability using the reluctivity with a prior knowledge of induction B instead of H, which is of in line with standard measurement systems. The complex permeability approach shows a significant reduction in computational time with reasonable level of accuracy as compared to the

existing approaches. The proposed magneto-elastic complex permeability is thereafter used to simulate the SST device under mechanical loading conditions. Computed losses are in close agreement with the measured losses.

An advantage of representing core material using complex permeability is that all loss components can be considered in a single function for a wide range of frequencies. The model can be applied successfully over a wide range of frequencies as the skin-effect phenomenon is taken into consideration. Reduction in computation time and simplicity are the main attractive features of the model. The model could also be extended to consider anisotropy, rotational flux, and multiaxial nature of induced mechanical stresses in practical devices [48], which is identified as a future work. Application of the model in FEM simulations of rotating machines has also been identified as a future work.

Data Availability

The measured data required to replicate these results cannot be shared at this time as the data also forms part of an ongoing work.

References

[1] R. M. Bozorth, Ferromagnetism, Van Norstand, New York, 1951 (1951).

[2] B. D. Cullity, C. D. Graham, Introduction to magnetic materials, John Wiley & Sons, 2011 (2011).

[3] L. Bernard, L. Daniel, Effect of stress on magnetic hysteresis losses in a switched reluctance motor: Application to stator and rotor shrink fitting, IEEE Transactions on Magnetics 51 (9) (2015) 1–13 (2015).

[4] A. Belahcen, Magnetoelastic coupling in rotating electrical machines, IEEE Transactions on Magnetics 41 (5) (2005) 1624–1627 (2005).

[5] A. Moses, Effects of stresses on magnetic properties of silicon-iron laminations, Journal of materials science 9 (2) (1974) 217–222 (1974).

[6] P. Baudouin, A. Belhadj, F. Breaban, A. Deffontaine, Y. Houbaert, Effects of laser and mechanical cutting modes on the magnetic properties of low and medium si content nonoriented electrical steels, IEEE transactions on magnetics 38 (5) (2002) 3213–3215 (2002).

[7] A. P. S. Baghel, J. B. Blumenfeld, L. Santandrea, G. Krebs, L. Daniel, Effects of mechanical stress on core losses along orthogonal directions in electrical steels, in: 18th International Symposium on Applied Electromagnetics and Mechanics (ISEM-2017), France, 2017 (2017).

[8] D. Miyagi, N. Maeda, Y. Ozeki, K. Miki, N. Takahashi, Estimation of iron loss in motor core with shrink fitting using fem analysis, IEEE Transactions on Magnetics 45 (3) (2009) 1704–1707 (2009).

[9] K. Fujisaki, R. Hirayama, T. Kawachi, S. Satou, C. Kaidou, M. Yabumoto, T. Kubota, Motor core iron loss analysis evaluating shrink fitting and stamping by finite-element method, IEEE Transactions on Magnetics 43 (5) (2007) 1950–1954 (2007).

[10] F. Ossart, E. Hug, O. Hubert, C. Buvat, R. Billardon, Effect of punching on electrical steels: Experimental and numerical coupled analysis, IEEE Transactions on Magnetics 36 (5) (2000) 3137–3140 (2000).

[11] A. Pulnikov, V. Permiakov, M. De Wulf, J. Melkebeek, Measuring setup for the investigation of the influence of mechanical stresses on magnetic properties of electrical steel, Journal of Magnetism and Magnetic Materials 254 (2003) 47–49 (2003).

[12] X. Liu, G. R. Slemon, An improved method of optimization for electrical machines, IEEE Transactions on Energy Conversion 6 (3) (1991) 492–496 (1991).

[13] S. Zeze, Y. Kai, T. Todaka, M. Enokizono, Vector magnetic characteristic analysis of a pm motor considering residual stress distribution with complex-approximated material modeling, IEEE Transactions on magnetics 48 (11) (2012) 3352–3355 (2012).

19

[14] Y. Xiao, P. Zhou, M. Rosu, Decoupled magnetoelastic finite element method including magnetostriction effects in electrical machinery applications, in: 2017 IEEE International Electric Machines and Drives Conference (IEMDC), IEEE, 2017, pp. 1–6 (2017).

[15] P. Rasilo, U. Aydin, D. Singh, F. Martin, R. Kouhia, A. Belahcen, A. Arkkio, Multiaxial magneto-mechanical modelling of electrical machines with hysteresis, in: 8th IET International Conference on Power Electronics, Machines and Drives (PEMD 2016), 2016, pp. 1–6 (April 2016). doi:10.1049/cp.2016.0183.

[16] K. Yamazaki, H. Mukaiyama, L. Daniel, Effects of multi-axial mechanical stress on loss characteristics of electrical steel sheets and interior permanent magnet machines, IEEE Transactions on Magnetics 54 (3) (2018) 1–4 (2018).

[17] D. C. Jiles, D. L. Atherton, Theory of ferromagnetic hysteresis, Journal of magnetism and magnetic materials 61 (1-2) (1986) 48–60 (1986).

[18] I. Mayergoyz, The classical preisach model of hysteresis and reversibility, Journal of Applied Physics 69 (8) (1991) 4602–4604 (1991).

[19] F. Henrotte, A. Nicolet, K. Hameyer, An energy-based vector hysteresis model for ferromagnetic materials, COMPEL-The international journal for computation and mathematics in electrical and electronic engineering 25 (1) (2006) 71–80 (2006).

[20] A. Bergqvist, G. Engdahl, A stress-dependent magnetic preisach hysteresis model, IEEE transactions on magnetics 27 (6) (1991) 4796–4798 (1991).

[21] A. Sipeky, A. Ivanyi, Preisach-type stress-dependent magnetic vector hysteresis model, Physica B: Condensed Matter 403 (2-3) (2008) 491–495 (2008).

[22] O. Bottauscio, A. Lovisolo, P. E. Roccato, M. Zucca, C. Sasso, R. Bonin, Modeling and experimental analysis of magnetostrictive devices: From the material characterization to their dynamic behavior, IEEE Transactions on Magnetics 44 (11) (2008) 3009–3012 (2008).

[23] T. Suzuki, E. Matsumoto, Comparison of jiles–atherton and preisach models extended to stress dependence in magnetoelastic behaviors of a ferromagnetic material, Journal of materials processing technology 161 (1-2) (2005) 141–145 (2005).

[24] M. J. Sablik, D. C. Jiles, Coupled magnetoelastic theory of magnetic and magnetostrictive hysteresis, IEEE transactions on magnetics 29 (4) (1993) 2113–2123 (1993).

[25] M. Sablik, H. Kwun, G. Burkhardt, D. Jiles, Model for the effect of tensile and compressive stress on ferromagnetic hysteresis, Journal of Applied physics 61 (8) (1987) 3799–3801 (1987).

[26] H. Naus, Theoretical developments in magnetomechanics, IEEE Transactions on Magnetics 47 (9) (2011) 2155–2162 (2011).

[27] L. Daniel, M. Rekik, O. Hubert, A multiscale model for magneto-elastic behaviour including hysteresis effects, Archive of Applied Mechanics 84 (9-11) (2014) 1307–1323 (2014).

[28] O. Hubert, L. Daniel, Multiscale modeling of the magneto-mechanical behavior of grain-oriented silicon steels, Journal of Magnetism and Magnetic Materials 320 (7) (2008) 1412–1422 (2008).

[29] E. Dlala, Comparison of models for estimating magnetic core losses in electrical machines using the finite-element method, IEEE Transactions on Magnetics 45 (2) (2009) 716–725 (2009).

[30] N. Sadowski, N. Batistela, J. Bastos, M. Lajoie-Mazenc, An inverse jiles-atherton model to take into account hysteresis in time-stepping finite-element calculations, IEEE Transactions on Magnetics 38 (2) (2002) 797–800 (2002).

[31] D. M. Ionel, M. Popescu, M. I. McGilp, T. Miller, S. J. Dellinger, R. J. Heideman, Computation of core losses in electrical machines using improved models for laminated steel, IEEE Transactions on Industry Applications 43 (6) (2007) 1554–1564 (2007).

[32] M. H. Gracia, E. Lange, K. Hameyer, Numerical calculation of iron losses in electrical machines with a modified post-processing formula, in:

Proceedings of the 16th International Symposium on Electromagnetic Fields COMPUMAG, Aachen, Germany, 2007 (2007).

[33] A. Belahcen, E. Dlala, K. Fonteyn, M. Belkasim, A posteriori iron loss computation with a vector hysteresis model, COMPEL-The international journal for computation and mathematics in electrical and electronic engineering 29 (6) (2010) 1493–1503 (2010).

[34] K. Ali, K. Atallah, D. Howe, Prediction of mechanical stress effects on the iron loss in electrical machines, Journal of applied physics 81 (8) (1997) 4119–4121 (1997).

[35] O. Saeed, A. Saleem, T. Rahman, R. Chromik, D. Lowther, Iron loss models under static stress for non-oriented and grain oriented steel, in: Proceedings of the 20th International Conference on the Computation of Electromagnetic Fields (Compumag), Montreal, 2015 (2015).

[36] J. Karthaus, S. Steentjes, N. Leuning, K. Hameyer, Effect of mechanical stress on different iron loss components up to high frequencies and magnetic flux densities, COMPEL-The international journal for computation and mathematics in electrical and electronic engineering 36 (3) (2017) 580–592 (2017).

[37] D. Singh, P. Rasilo, F. Martin, A. Belahcen, A. Arkkio, Effect of mechanical stress on excess loss of electrical steel sheets, IEEE Transactions on Magnetics 51 (11) (2015) 1–4 (2015).

[38] H. Tavakoli, D. Bormann, D. Ribbenfjärd, G. Engdahl, Comparison of a simple and a detailed model of magnetic hysteresis with measurements on electrical steel, COMPEL-The international journal for computation and mathematics in electrical and electronic engineering 28 (3) (2009) 700–710 (2009).

[39] A. P. S. Baghel, S. V Kulkarni, Modeling of magnetic characteristics including hysteresis effects for transformers, in: 3 rd International Colloquium Transformer Research and Asset Management Split, 2014 (10 2014).

[40] K. P. Badgujar, A. Baghel, S. Kulkarni, A coupled field-circuit formulation and a duality based approach for analysis of low-frequency response

of transformers, in: 2013 Annual IEEE India Conference (INDICON), IEEE, 2013, pp. 1–6 (2013).

[41] N. Abeywickrama, Y. V. Serdyuk, S. M. Gubanski, High-frequency modeling of power transformers for use in frequency response analysis (fra), IEEE transactions on power delivery 23 (4) (2008) 2042–2049 (2008).

[42] S. D. Mitchell, J. S. Welsh, Modeling power transformers to support the interpretation of frequency-response analysis, IEEE Transactions on power delivery 26 (4) (2011) 2705–2717 (2011).

[43] K. Macfadyen, Vector permeability, Journal of the Institution of Electrical Engineers-Part III: Radio and Communication Engineering 94 (32) (1947) 407–414 (1947).

[44] V. Subbarao, Eddy currents in linear and non-linear media, Omega Scientific Publishers, New Delhi, 1991 (1991).

[45] K. Abeywickrama, A. D. Podoltsev, Y. V. Serdyuk, S. M. Gubanski, Computation of parameters of power transformer windings for use in frequency response analysis, IEEE Transactions on Magnetics 43 (5) (2007) 1983–1990 (2007).

[46] S. V. Kulkarni, S. A. Khaparde, Transformer engineering: design, technology, and diagnostics, CRC press, 2016 (2016).

[47] E. Dlala, A. Belahcen, A. Arkkio, A fast fixed-point method for solving magnetic field problems in media of hysteresis, IEEE Transactions on Magnetics 44 (6) (2008) 1214–1217 (2008).

[48] L. Daniel, O. Hubert, An equivalent stress for the influence of multiaxial stress on the magnetic behavior, Journal of Applied Physics 105 (7) (2009) 07A313 (2009).

[49] M. Rekik, L. Daniel, O. Hubert, Equivalent stress model for magnetic hysteresis losses under biaxial loading, IEEE Transactions on Magnetics 50 (4) (2014) 1–4 (2014).